7-13-2010

Development of daily precipitation projections for the United States based on probabilistic downscaling

Justin T. Schoof
Southern Illinois University Carbondale, jschoof@siu.edu

SC Pryor

J Surprenant
Southern Illinois University Carbondale

Recommended Citation
Schoof, Justin T., Pryor, SC and Surprenant, J. "Development of daily precipitation projections for the United States based on probabilistic downscaling." *Journal of Geophysical Research* 115 (Jul 2010). doi:doi:10.1029/2009JD013030.

JOURNAL OF GEOPHYSICAL RESEARCH, VOL. 115, D13106, doi:10.1029/2009JD013030, 2010

Development of daily precipitation projections for the United States based on probabilistic downscaling

J. T. Schoof,[1] S. C. Pryor,[2] and J. Surprenant[1]

Received 18 August 2009; revised 20 January 2010; accepted 31 March 2010; published 13 July 2010.

[1] Projections of mid and late 21st century precipitation for 963 stations across the contiguous United States are derived using probabilistic downscaling of 10 coupled atmosphere-ocean general circulation models (AOGCMs). The projections are constructed by downscaling the statistical parameters describing precipitation occurrence and intensity, using a first-order Markov chain and two-parameter gamma distribution, respectively. Future downscaled values of the parameters are used to derive projections of wet day probability, wet day precipitation intensity and its distribution, and total seasonal precipitation for the cold season (November through March) and the warm season (May through September). Downscaled results for the 10 AOGCMs indicate several robust features of possible changes in the U.S. regional precipitation climatology. Cold season projections are characterized by increases in precipitation in the northwest and northeast regions, decreases in precipitation in the southwest region, and smaller or inconsistent changes in other regions. With the exception of the northeast region, warm season projections reflect drier conditions overall resulting primarily from fewer wet days. In both the cold and warm seasons, changes in both the occurrence and intensity processes contribute to changes in total precipitation. Changes in total precipitation, and the relative roles of the occurrence and intensity processes, are found to be sensitive to the change in the distribution of wet day precipitation intensities. Regions with increasing seasonal precipitation totals are characterized by disproportionate increases in large precipitation events, while those with decreasing seasonal precipitation totals are characterized by the largest fractional decreases in small precipitation events.

Citation: Schoof, J. T., S. C. Pryor, and J. Surprenant (2010), Development of daily precipitation projections for the United States based on probabilistic downscaling, *J. Geophys. Res.*, *115*, D13106, doi:10.1029/2009JD013030.

1. Introduction

[2] At the global scale annual total precipitation over land does not exhibit a significant trend over the last century [*Mitchell and Jones*, 2005; *Peterson and Vose*, 1997; *Trenberth et al.*, 2007]. At the regional scale, however, significant changes in both annual and seasonal precipitation and their characteristics have been documented. In the contiguous USA, there has been a 10% increase in annual precipitation increase since 1910 [*Karl and Knight*, 1998], with increases of 7–15% in all seasons except winter [*Groisman et al.*, 2001]. Increases in the annual frequency of wet days and heavy precipitation days and in the mean daily and annual precipitation in the USA during the last half-century have also been documented though with regional variability [*Higgins et al.*, 2007], and robust trends in extreme precipitation metrics have also been reported [*Groisman et al.*, 2005; *Pryor et al.*, 2009]. Furthermore, over many land regions, even those where annual precipitation has decreased, extreme precipitation has increased [*Trenberth et al.*, 2007]. Attribution of precipitation changes to anthropogenic forcing [*Zhang et al.*, 2007] and interest in mitigating and adapting to changes in extreme precipitation [*Allen and Soden*, 2008; *Hennessy et al.*, 1997; *Karl et al.*, 2009; *Kharin et al.*, 2007] has spurred interest in further development of regional precipitation projections for climate change scenarios.

[3] The primary tools for investigating evolution of the climate system under different forcing scenarios are coupled atmospheric-oceanic general circulation models, or AOGCMs. However, the relatively coarse resolution of AOGCMs and the parameterizations employed limits the realism of the daily precipitation time series produced by AOGCMS [*Liang et al.*, 2006]. AOGCMs have a tendency to simulate too many wet days [*Schoof et al.*, 2009], and one study of 18 coupled AOGCMs found that spatial patterns of precipitation frequency and intensities were not well simulated, with most models overestimating the frequency of small events and underestimating the precipitation intensities for large events [*Sun et al.*, 2006]. Similarly precipitation in AOGCM simu-

[1]Department of Geography and Environmental Resources, Southern Illinois University, Carbondale, Illinois, USA.
[2]Atmospheric Science Program, Department of Geography, Indiana University, Bloomington, Indiana, USA.

0148-0227/10/2009JD013030

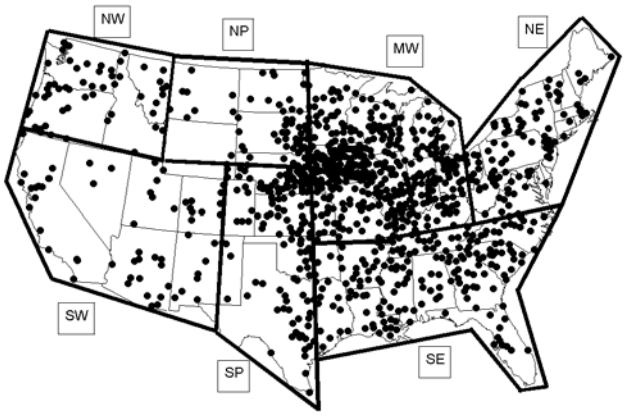

Figure 1. Map of the surface observing stations used in this study. Also shown are the seven regions for which results are summarized: Northwest (NW), Southwest (SW), Northern Plains (NP), Southern Plains (SP), Midwest (MW), Southeast (SE), and Northeast (NE).

lations for western North America exhibits a positive bias [*Christensen et al.*, 2007]. The result of these shortcomings is that although total seasonal or annual precipitation may be reproduced in the model simulations, the characteristics of daily precipitation are not. The surface hydrologic response to precipitation depends critically on the nature (both occurrence and intensity) of daily precipitation, as well as the total amount [*Trenberth et al.*, 2003]. Assessment of potential climate change impacts, such as those in agriculture [*Rosenzweig et al.*, 2002], also require realistic daily precipitation characteristics and totals. These studies and others draw attention to the need to better understand the interaction between precipitation occurrence and precipitation intensity and how changes in either metric are likely to impact overall precipitation receipt under global warming scenarios.

[4] The need for realistic climate change information at small spatial scales has led to the development of downscaling techniques. Differences between precipitation estimates from AOGCMs may be due to differences in their precipitation parameterizations rather than differences in the large scale conditions that partially govern precipitation [*Hewitson and Crane*, 2006]. This notion is also supported by the work of *Wilby and Wigley* [2000], who found that observed and AOGCM-simulated relationships between large-scale circulation and precipitation were inconsistent, suggesting that model precipitation processes are inherently flawed. In this context, downscaling serves as the link between the well-simulated large-scale climate and poorly simulated precipitation series. For reasons already articulated, precipitation downscaling methods must be able to address both occurrence and intensity to be considered useful to the climate change impacts community. Stochastic modeling provides a framework for addressing the evolution of multiple precipitation characteristics (occurrence and intensity) under enhanced greenhouse gas forcing assuming that the model parameters can be adjusted in a manner consistent with the climate change signal produced by the AOGCM.

[5] Downscaling with stochastic models was originally proposed by *Wilks* [1992] and this approach has consistently performed well relative to other methods [*Wetterhall et al.*, 2006]. Approaches to downscaling with stochastic weather generators vary primarily in the way that the parameters are perturbed to reflect the changed climate. Most commonly, weather typing approaches or airflow descriptors have been employed to condition the weather generator [*Stehlik and Bardossy*, 2002; *Vrac and Naveau*, 2007; *Wilby et al.*, 2002]. Less commonly, statistical parameters have been derived from large scale fields via regression methods or other statistical means [*Cannon*, 2008; *Schoof et al.*, 2007, 2009] or simply scaled according to their AOGCM counterparts.

[6] In this study, we present a new approach to downscaling daily precipitation and use it to downscale 10 of the CMIP3 AOGCMs [*Meehl et al.*, 2007]. The downscaling approach is based on extension of the probabilistic downscaling method introduced by *Pryor et al.* [2005] to stochastic weather generator parameters. Using our new approach we investigate the evolution of daily precipitation occurrence and intensity parameters, providing a framework for investigating regional changes in precipitation climates. Given the framework, our study addresses the question of whether changes in total precipitation are likely to occur under enhanced greenhouse gas forcing and whether such changes will result from changes in precipitation occurrence (i.e., the number of wet days), intensity (i.e., the amount of precipitation on those days), or a combination of both. To our knowledge, this is the first study to apply probabilistic downscaling to stochastic weather generator parameters and develop precipitation projections for sites across the USA based on multiple AOGCMs. In section 2, we describe the data sets used in the analysis. In section 3, a description of the methods is presented. The results are described in section 4 and concluding remarks follow in section 5.

2. Data and Models

[7] Historical daily precipitation data are drawn from the data set developed by *Kunkel et al.* [1998, 2005] and the National Weather Service Cooperative Observing Program (COOP) archive, and are used to investigate recent changes in the precipitation occurrence and intensity processes, train and validate the downscaling models, and provide a context for model simulated changes. While some station records extend to 1888, we limit our analysis to the period from 1961 to 2000, in which a large number of stations have records that are nearly complete and matching AOGCM simulations are also available. Although the data have undergone a quality control procedure, we additionally discard any station with fewer than 360 valid observations within any calendar year in the period 1961–2000. This results in a total of 963 stations used in the analysis (Figure 1). To synthesize the downscaling analyses, the results are presented in seven regions similar to those used in previous regional climate change assessments and in a previous study focused on changes in precipitation seasonality [*Pryor and Schoof*, 2008] (Figure 1).

[8] To investigate the relationship between daily precipitation and large scale (upper level) predictors we employ a suite of variables on a 2.5° × 2.5° grid extracted from the European Center for Medium Range Weather Forecasting (ECMWF) ERA-40 reanalysis product [*Uppala et al.*, 2005]. The precipitation projections are derived based

on daily output from ten AOGCMs from the CMIP3 model archive: BCCR BCM2.0, CCCMa CGCM3.1, CNRM CM3, CSIRO Mk3.0, GFDL CM2.0, GISS Model E Russell, IPSL CM4, MIUB ECHO G, MPI ECHAM5, and MRI CGCM2.3.2a (see *Meehl et al.* [2007] and http://www-pcmdi.llnl.gov/ipcc/model_documentation/ipcc_model_documentation.php). These models span a range of spatial resolutions (from approximately 4° × 5° to approximately 1.9° × 1.9°) and model formulations (e.g., spectral versus grid-cell). All of the model output is interpolated to a standard 2.5° × 2.5° grid corresponding to the ECMWF reanalysis data. AOGCM output is available for three periods: 1961–2000, 2046–2065, and 2081–2100. The 20th century period is used to evaluate the ability of the models to reproduce observed precipitation occurrence and intensity statistics when used directly and when downscaled. The 21st century model data are from simulations conducted under the SRES A2 emissions scenario [*Nakicenovic and Swart*, 2000]. This scenario equates to a moderate to high cumulative carbon emission resulting in global carbon dioxide emissions in 2100 that are around four times the 1990 value.

3. Methodology

3.1. Daily Precipitation Model and Derived Quantities

3.1.1. Daily Precipitation Occurrence

[9] Daily precipitation occurrence is a binary variable; a day is either wet (1) or dry (0). Although several statistical models for daily precipitation occurrence have been proposed, the first-order Markov chain has been the most widely applied. A recent assessment of model order, found that for most U.S. stations and months, the 1st order model successfully reproduces the observed precipitation occurrence climatology, including the distributions of dry and wet spells [*Schoof and Pryor*, 2008]. For the first-order Markov model, the precipitation occurrence process is fully defined by two transition probabilities: p_{01} (the probability of a wet day following a dry day) and p_{11} (the probability of a wet day following a wet day). Maximum likelihood estimates of p_{01} and p_{11} can be readily computed from observed data [*Wilks*, 2006]. The resulting wet day probability is given by $\pi = p_{01}/(1 + p_{01} - p_{11})$. A precipitation occurrence series is generated by producing a uniform [0,1] random number. If the number is less than the appropriate transition probability (p_{01} if the previously generated day was dry or p_{11} if the previously generated day was wet), a wet day is generated. Otherwise, a dry day is generated.

3.1.2. Daily Precipitation Intensity

[10] Although several statistical distributions have been proposed for wet day precipitation intensities [*Wilks*, 1999], the gamma distribution has been the most widely applied. The gamma probability distribution function is given by:

$$f(x) = \frac{\left(\frac{x}{\beta}\right)^{\alpha-1} e^{\left[\frac{-x}{\beta}\right]}}{\beta\Gamma(\alpha)}, x, \alpha, \beta > 0 \quad (1)$$

where x is the daily precipitation intensity, α and β are the gamma shape and scale parameters, respectively, and $\Gamma(\alpha)$ is the gamma function evaluated at α. The mean and variance of wet day precipitation intensities are given by $\alpha\beta$ and $\alpha\beta^2$, respectively. Stochastic generation of daily precipitation time series can be accomplished by randomly drawing a precipitation intensity value from the gamma distributions on each simulated wet day.

3.2. Downscaling Approach

[11] Application of the daily precipitation model described above to AOGCM output requires that the four parameters (p_{01}, p_{11}, α, and β) be downscaled with dependence on the large scale climate. Once downscaled, the four parameters can be used to derive the overall wet day probability (π), the mean wet day intensity ($\alpha\beta$) and the total precipitation for any time period of interest ($n\pi\alpha\beta$), where n is the number of days in the time period.

3.3. Model Construction and Validation

[12] Regression models were constructed separately for p_{01}, p_{11}, α, and β and for each of the 963 stations shown in Figure 1. AOGCM skill varies considerable among variables, AOGCMs and temporal and spatial scales [*Benestad et al.*, 2008], and there is some evidence that AOGCM results diverge at the smallest spatial scales [*Grotch and MacCracken*, 1991]. We therefore adopt a conservative approach that uses model output at the scale of several grid boxes. For each station, the large-scale predictor data are averaged over the grid box in which the station resides and two grid boxes in each cardinal direction. This results in a 12.5° × 12.5° regional average for each predictor. Additionally, because the AOGCMs may exhibit bias relative to reanalysis data, all of the downscaling equations are constructed using anomalies. When applied to future periods, the AOGCM anomalies are computed using the 1961–2000 as the reference period.

[13] Considerable efforts have been made to identify optimal predictors for precipitation in the context of downscaling [*Cavazos and Hewitson*, 2005; *Wilby and Wigley*, 2000]. Predictors must not only contribute to precipitation variability in the current climate, but also reflect likely changes in precipitation under enhanced greenhouse gas conditions. For example, analysis using the continuity equation for atmospheric moisture has been used to demonstrate that sea level pressure only partially contributes to precipitation variability [*Benestad et al.*, 2008]. *Cavazos and Hewitson* [2005] identified mid-tropospheric heights and humidity as the best predictors of daily precipitation, but also cautioned that the optimal predictors may be regionally specific. *Wetterhall et al.* [2006] additionally identified humidity as a contributor to improved modeling of interannual variability of precipitation. Future changes in precipitation in midlatitude regions are likely to depend strongly on increased water vapor transport to regions of moisture convergence [*Meehl et al.*, 2005] and changes in surface pressure associated with a poleward shift in storm tracks [*Yin*, 2005].

[14] Based on these studies, a large number of predictors were considered for inclusion in the models including zonal and meridional wind speed, specific humidity, air temperature (all at three levels: 500 mbar, 700 mbar, and 850 mbar), as well as sea level pressure. For each of the regions (Figure 1), regionally consistent variables were chosen that minimized the regionally averaged mean absolute relative error (MARE; %) using a model cross-validation procedure. In this cross-

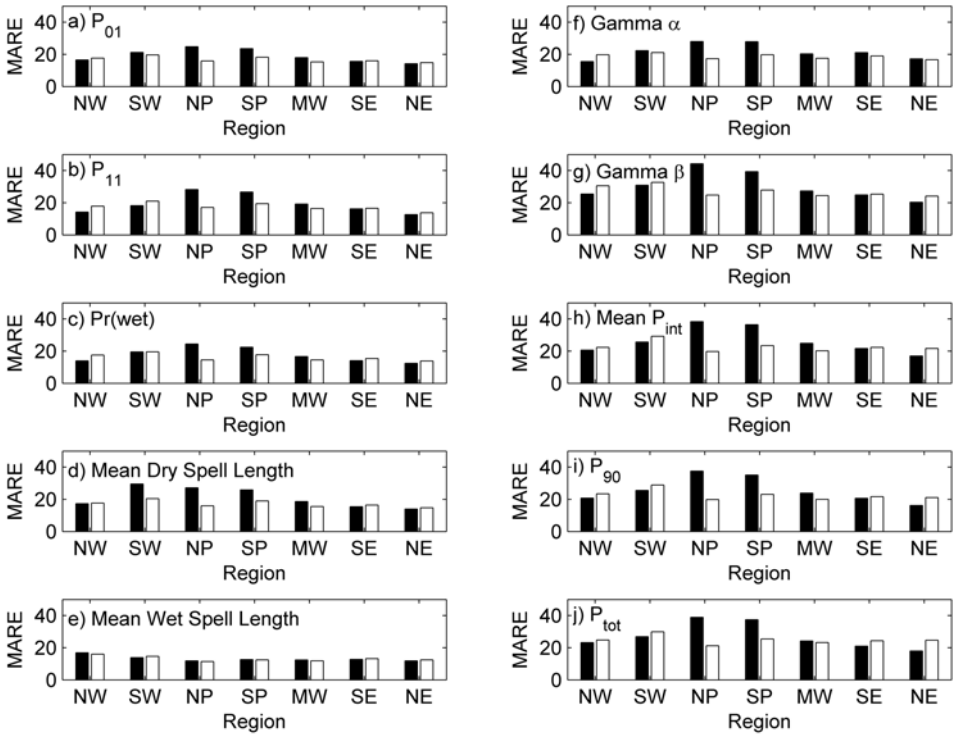

Figure 2. Mean absolute relative error (MARE, %) for seasonal mean daily precipitation characteristics: (a) transition probability p_{01}, (b) transition probability p_{11}, (c) wet day probability, (d) mean dry spell length, (e) mean wet spell length, (f) the gamma shape parameter (α), (g) the gamma scale parameter (β), (h) wet day precipitation intensity (P_{int}), (i) the 90th percentile of wet-day precipitation (P_{90}), and (j) total seasonal precipitation (P_{tot}). The black bar corresponds to the cold season (November through March), and the white bar corresponds to warm season (May through September). The validation period is 1987 to 2000.

validation data from 1961 to 1986 were used for the model training, while data from 1987 to 2000 were used for validation. The predictors that resulted in the lowest MARE when applied to the ECMWF reanalysis data and evaluated using independent data were chosen for inclusion in the final models (Table 1 and Figure 2).

[15] The MARE values for the validation exercise are presented in Figure 2 and are smaller in magnitude than the inter-annual variability (measured simply as the coefficient of variation of the seasonal values) in all cases, demonstrating skill in the downscaling procedure for the validation period. Although warm season (May through September) precipitation is traditionally predicted with lower skill than cold season precipitation, the validation exercise (Figure 2) suggests that the downscaled seasonal totals exhibit considerably higher skill during the warm season in the Northern and Southern Plain regions. However, the large MARE values in the NP and SP regions during the cold season and in the SW region during the warm season are associated with small absolute errors since these regions are relatively dry during these seasons resulting in smaller values of the model parameters (p_{01}, p_{11}, α and β). Extension of the downscaled parameters to derived variables (e.g., 90th percentile of wet day precipitation, mean dry/wet spell length) provides additional confidence in the model for climate projection. Consistent with previous precipitation downscaling studies [*Haylock et al.*, 2006], precipitation occurrence is generally downscaled with greater skill than precipitation intensity (Figure 2).

4. Results

[16] The optimal downscaling model parameters derived from the validation procedure described in section 3.3 were

Table 1. Downscaling Predictors for Region and Predictand for Cold Season and Warm Season[a]

	P_{01}	P_{11}	Gamma α	Gamma β
Cold Season (November Through March)				
Northwest (NW)	Q_{700}, T_{700}	SLP, U_{500}	T_{700}, U_{700}	Q_{500}, U_{500}
Southwest (SW)	Q_{700}, T_{700}	Q_{700}, T_{500}	T_{700}, V_{700}	Q_{700}, V_{700}
Northern Plains (NP)	Q_{700}, T_{700}	U_{700}, V_{500}	SLP, T_{500}	SLP, U_{700}
Southern Plains (SP)	Q_{700}, T_{700}	U_{700}, V_{500}	T_{500}, U_{700}	SLP, V_{700}
Midwest (MW)	T_{700}, V_{700}	Q_{700}, T_{500}	Q_{500}, T_{500}	SLP, Q_{700}
Southeast (SE)	Q_{700}, V_{700}	Q_{700}, V_{500}	Q_{500}, T_{500}	SLP, V_{700}
Northeast (NE)	T_{700}, V_{700}	Q_{700}, T_{500}	T_{500}, U_{500}	Q_{500}, U_{700}
Warm Season (May Through September)				
Northwest (NW)	Q_{700}, T_{700}	SLP, U_{500}	SLP, V_{700}	SLP, V_{500}
Southwest (W)	Q_{700}, T_{700}	Q_{700}, T_{500}	SLP, U_{700}	U_{700}, V_{700}
Northern Plains (NP)	Q_{700}, U_{500}	T_{700}, V_{500}	SLP, Q_{500}	SLP, V_{500}
Southern Plains (SP)	T_{700}, U_{500}	Q_{700}, U_{500}	SLP, T_{500}	Q_{700}, U_{500}
Midwest (MW)	U_{500}, V_{500}	SLP, V_{500}	SLP, Q_{700}	T_{500}, U_{500}
Southeast (SE)	Q_{500}, T_{700}	Q_{700}, V_{500}	Q_{700}, U_{700}	SLP, V_{700}
Northeast (NE)	Q_{700}, V_{700}	Q_{700}, U_{700}	SLP, Q_{500}	Q_{700}, U_{700}

[a]The same predictor variables were used for all individual stations within a region.

Table 2. Changes in Cold Season and Warm Season Precipitation Occurrence, Amount, and Seasonal Total Expressed as Percentage Differences Computed From (Future – Current)/Current (1961–2000) Values[a]

Region	Period	Pr(wet)	Mean P_{int}	P_{10}	P_{50}	P_{90}	P_{tot}
			Cold Season (November Through March)				
NW	1	0.4	**9.7 (85.6)**	*3.9 (62.7)*	**8.3 (80.0)**	**10.5 (87.6)**	**10.2 (81.6)**
	2	1.2	**20.4 (83.6)**	**6.5 (57.8)**	**16.7 (77.5)**	**22.4 (86.7)**	**20.0 (82.6)**
SW	1	**−19.8 (86.3)**	*5.2 (64.3)*	*6.2 (56.4)*	*4.9 (62.5)*	*5.1 (65.5)*	*−15.1 (73.2)*
	2	*−31.0 (87.5)*	*14.2 (66.1)*	**23.4 (57.3)**	*14.1 (62.3)*	*13.5 (66.4)*	*−21.1 (76.1)*
NP	1	**−6.0 (65.9)**	0.1	−1.1	−1.0	0.6	−7.0
	2	−5.2	−1.34	*8.8 (55.2)*	−2.1	−1.6	*−11.1 (65.7)*
SP	1	−0.7	−3.2	**−6.4 (62.0)**	**−5.2 (60.5)**	−2.3	−4.7
	2	*6.3 (59.1)*	**−8.0 (62.5)**	0.4	**−10.8 (62.9)**	**−7.5 (62.0)**	−6.1
MW	1	**−4.5 (64.5)**	*10.8 (71.3)*	**8.0 (55.1)**	*9.1 (65.1)*	*11.6 (74.7)*	*4.9 (64.1)*
	2	**−8.5 (64.5)**	**19.8 (69.2)**	**21.4 (62.7)**	**15.6 (61.3)**	**21.1 (74.4)**	4.9
SE	1	*7.0 (85.5)*	**−4.4 (62.9)**	**−11.8 (65.8)**	**−7.1 (64.5)**	**−3.5 (62.2)**	*2.1 (54.6)*
	2	*18.4 (85.3)*	**−10.8 (66.9)**	**−14.2 (52.9)**	**−15.4 (67.0)**	**−9.6 (67.0)**	4.6
NE	1	*3.7 (62.3)*	**12.1 (88.4)**	**8.9 (62.6)**	*11.1 (80.5)*	**12.5 (91.6)**	*16.0 (88.9)*
	2	*8.7 (64.4)*	**26.8 (90.9)**	**24.4 (65.0)**	**24.7 (80.9)**	**27.6 (93.8)**	**36.6 (92.3)**
			Warm Season (May Through September)				
NW	1	**−24.6 (93.1)**	0.7	−0.8	0.3	0.9	**−24.3 (92.0)**
	2	**−37.4 (90.7)**	1.4	−1.3	0.6	1.8	**−36.7 (90.0)**
SW	1	**−10.9 (77.1)**	−0.4	−0.3	−0.5	−0.3	*−11.0 (75.3)*
	2	*−13.0 (70.0)*	−0.7	0.2	−0.9	−0.7	−13.
NP	1	**−3.4 (64.4)**	**−1.0 (51.1)**	2.1	**−1.4 (51.6)**	**−1.1 (50.3)**	**−5.1 (68.7)**
	2	**−6.2 (64.1)**	*−1.5 (51.4)*	*16.1 (50.3)*	−1.3	**−2.5 (51.3)**	**−10.3 (71.3)**
SP	1	**−20.7 (94.2)**	*−2.3 (54.7)*	**18.0 (53.1)**	*−1.2 (53.8)*	**−3.2 (55.6)**	**−23.8 (87.1)**
	2	**−36.4 (93.8)**	**−3.0 (58.0)**	**49.3 (53.5)**	0.0	**−5.6 (60.0)**	**−40.8 (89.9)**
MW	1	−2.6	**7.1 (64.6)**	**3.2 (50.6)**	**5.4 (61.0)**	**7.7 (65.9)**	*4.4 (60.0)*
	2	*−5.8 (83.8)*	**9.7 (60.1)**	**6.6 (56.1)**	**5.8 (54.6)**	**11.1 (62.4)**	3.7
SE	1	**−22.4 (95.2)**	*−3.1 (59.6)*	*−4.7 (57.1)*	*−4.1 (58.7)*	*−2.8 (60.1)*	**−25.7 (98.5)**
	2	**−37.0 (92.9)**	*−6.6 (61.8)*	−2.7	**−8.1 (60.5)**	*−6.3 (62.4)*	**−44.1 (98.1)**
NE	1	*8.0 (80.5)*	*3.9 (64.9)*	*−7.0 (52.3)*	0.3	**5.4 (70.2)**	**11.6 (82.3)**
	2	**20.1 (86.6)**	**6.7 (62.1)**	**−7.9 (57.7)**	−1.2	**9.6 (66.1)**	**24.8 (82.3)**

[a]Period 1 and Period 2 refer to 2046–2065 and 2081–2100, respectively. Bold entries indicate cases in which all 10 downscaled AOGCMs agree on the sign of change. Italicized entries indicate cases in which 9 of the 10 downscaled AOGCMs agree. For regions and descriptors that exhibit consistency among downscaled AOGCMs, the number in parentheses indicates the percentage of regional stations that agree on the sign of the projected change. Pr(wet), precipitation occurrence; precipitation amount: P_{int}, mean; P_{10}, 10th percentile; P_{50}, 50th percentile; and P_{90}, 90th percentile; and P_{tot}, seasonal total.

applied to the three periods for which AOGCM output is available to assess possible future evolution of daily precipitation occurrence and intensity, and their contributions to total seasonal precipitation. Regression equations were thus developed and applied to each of the 963 stations for each of the 10 AOGCMs to derive seasonal values of the transition probabilities (p_{01}, p_{11}), the gamma shape and scale parameters (α and β) and the derived values (wet day probability, wet day precipitation intensity, and total seasonal precipitation). The average change (difference) in each of these parameters for the future time periods relative to the historical control (1961–2000) was calculated for each AOGCM and station combination. For reporting purposes, the station-level results were synthesized in each of the regions depicted in Figure 1. For all variables, changes are reported for the cold season (November through March) and the warm season (May through September) and expressed as percentages of the 1961–2000 observed values. The detailed results are presented in Table 2, which shows the change in wet-day occurrence, mean wet-day precipitation intensity, 10th, 50th, and 90th percentiles of wet-day precipitation intensity, and total seasonal precipitation. A brief interpretation of these results is given in the following subsections.

4.1. Precipitation Occurrence

[17] It has been reported that a general response to greenhouse gas forcing manifest in AOGCMs is a reduction in the frequency of precipitation over most land areas [*Semenov and Bengtsson*, 2002]. However, our regional projections indicate the presence of both regions characterized by coherent increases and regions where declines dominate (Table 2 and Figure 3).

4.1.1. Cold Season

[18] Downscaling results for the cold season (NDJFM) indicate that the Southwest region is characterized by a decline in the frequency of wet days of −20% in 2046–2065 and more than 30% in 2081–2100. This signal is consistent among over 86% of stations within the region, and all downscaled AOGCMs except IPSL CM4 in the latter period (2081–2100). Closer inspection reveals that the regional sea level pressure projections from IPSL CM4 are the lowest among the models used here. The downscaled AOGCM projections also reflect consistent, but smaller magnitude, decreases in wet day probability (around −5% and −8% for 2046–2065 and 2081–2100, respectively) for the Midwest region (Table 2 and Figure 3). Conversely, downscaled precipitation occurrence for the future periods is characterized by increases in the Southern Plains, Southeast and Northeast regions, with the exception of downscaling from the CSIRO Mk3.0 model, although the consistency at the station-level varies considerably among the downscaled AOGCMs. The CSIRO Mk3.0 AOGCM exhibits very low mid-tropospheric specific humidity relative to the multi-

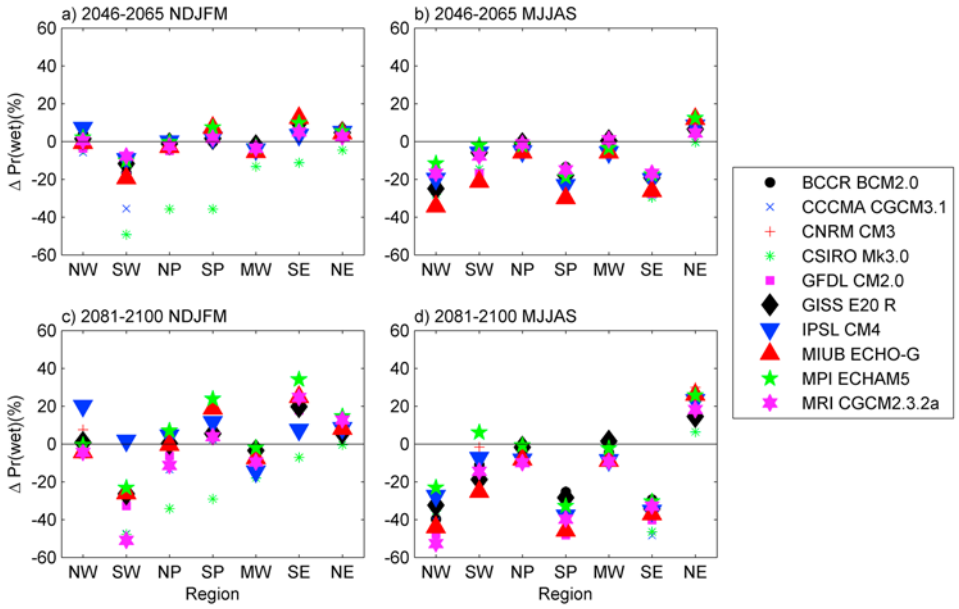

Figure 3. Projections of wet day probability change for (a, c) cold season (November through March) and (b, d) warm season (May through September) and for 2046–2065 (Figures 3a and 3b) and 2081–2100 (Figures 3c and 3d) relative to 1961–2000. Changes are shown as percentages of the 1961–2000 values averaged over all the stations in each region.

model ensemble, resulting in large negative changes in precipitation occurrence in several regions (Figure 3). In the Southern Plains, the ensemble average projected changes in precipitation occurrence are close to zero for the mid-century period, but approximately +6% for the late 21st century. For the Southeast region, projected changes in wet day probability for 2046–2065 and 2081–2100 are around +7% and +18%, respectively. For the Northeast region, the corresponding changes are +4% and +9%. Downscaled projections for the Northwest and Northern Plains regions generally exhibit small changes in precipitation occurrence with inconsistent sign among the AOGCMs used.

4.1.2. Warm Season

[19] Changes in warm season precipitation occurrence changes are more consistent among the regions, the stations within the regions, and the downscaled AOGCMs and, with the exception of the Northeast region indicate an overall decrease in precipitation occurrence under the A2 SRES (Table 2 and Figure 3). This result suggests that projections of annual decreases in precipitation occurrence previously reported [*Sun et al.*, 2007] are being driven primarily by changes in the warm season. Based on the downscaling presented herein, the largest decreases in warm season precipitation occurrence are projected to occur in the Northwest, Southern Plains, and Southeast regions (Table 2 and Figure 3) with changes of over −20% and −35% for 2046–2065 and 2081–2100, respectively. These changes are also consistent among the AOGCMs downscaled and stations with the regions, with all downscaled AOGCMs indicating declines in the regional mean precipitation frequency, and at least 75% of the stations in these regions indicating decreases for all of the downscaled AOGCMs. Decreases in precipitation occurrence are also projected for the Southwest, Northern Plains, and Midwest, but the level of consistency among AOGCMs and stations, as well as the magnitude of the projected changes is lower than that reported for the Northwest, Southern Plains, and Southeast. The Northeast region is an exception to the otherwise consistent decrease in wet day occurrence during the warm season. In this region, the downscaled AOGCMs indicate an increase in wet day occurrence during the warm season of approximately +8% by 2046–2065 and +20% by 2081–2100 with a high level of consistency among the stations within the region (>80%).

4.2. Precipitation Intensity

[20] Recent studies [*Pryor et al.*, 2009] have identified disproportionate increases in precipitation extremes using a variety of metrics. Therefore, in addition to mean wet day precipitation intensity (P_{int}) computed as the product of the gamma shape (α) and scale (β) parameters, we also consider changes in the shape of the distribution of wet day precipitation intensities for each downscaled AOGCM and station using the derived gamma distribution parameters. As discussed below, for both the cold season (NDJFM) and warm season (MJJAS), projections of the various metrics of precipitation intensity derived from downscaling of the 10 AOGCMs are consistent within several U.S. regions (Figures 4–6 and Table 2).

4.2.1. Cold Season

[21] The most notable characteristics of the cold season precipitation intensity projections is a consistent (among AOGCMs) increase for the Northwest, Southwest, Midwest, and Northeast regions. For these regions, at least 9 of 10 downscaled AOGCMs (CSIRO Mk3.0 is an outlier as in the precipitation occurrence analysis) agree on the sign of change for both projection periods (Table 2 (cold season)

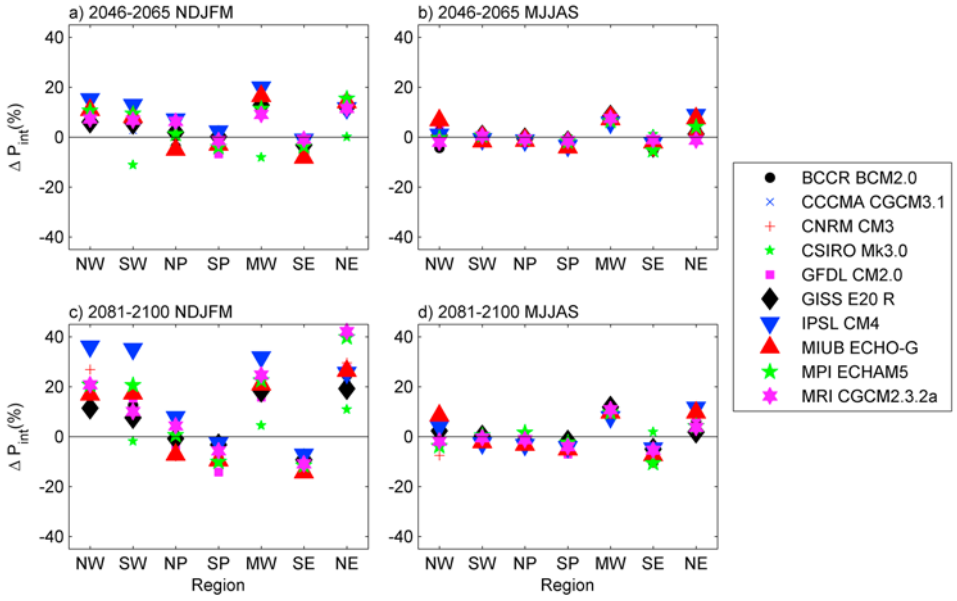

Figure 4. Projections of mean wet day precipitation intensity change for (a, c) cold season (November through March) and (b, d) warm season (May through September) and for 2046–2065 (Figures 4a and 4b) and 2081–2100 (Figures 4c and 4d) relative to 1961–2000. Changes are shown as percentages of the 1961–2000 values averaged over all the stations in each region.

and Figures 4 and 5). Projections for the Northwest and Northeast regions additionally exhibit strong regional coherence as manifest in the large number of stations within these regions that exhibit increased mean daily accumulated precipitation. For the Southwest and Midwest regions, approximately 70% of the stations exhibit agreement with respect to the sign of the projected change, which is positive in both cases. In all four of these regions, precipitation intensity projections are characterized by larger changes in the upper tail of the probability distribution as manifest in the larger fractional changes in P_{90} than mean P_{int} (Table 2) and large changes in the upper percentiles (Figure 5), in accord with historical studies that have identified robust changes in extreme precipitation over the 20th century [*Groisman et al.*, 2005; *Pryor et al.*, 2009].

[22] The downscaled and regionally averaged AOGCM projections indicate declines in mean P_{int} in both the Southern Plains and Southeast regions, although the level of agreement among stations within these regions is lower than that for the other regions. For the Southeast region, these changes exhibit a high level of consistency among all 10 downscaled AOGCMs (Figure 4). Inspection of the changes across the distribution of wet day precipitation intensities in these regions (SP and SE) indicate that although the largest precipitation intensities are projected to exhibit smaller fractional declines than moderate and small precipitation intensities (i.e., P_{50} and P_{10}) (Table 2), some of the downscaled AOGCMs do exhibit considerable declines in upper-tail precipitation intensities (Figure 5).

4.2.2. Warm Season

[23] The downscaled mean wet day precipitation intensity during the warm season generally exhibit smaller changes than their cold season counterparts (Figure 4) with less consistency among the AOGCMs and among stations within each region. The Northern Plains and Southern Plains regions are characterized by small regionally averaged projected changes of up to −3%, but with consistent sign among the AOGCMs for the mean wet day precipitation intensity. For both regions, the changes are characterized by an increase in the 10th percentile and a decrease in the 90th percentile, indicating a reduction in the variance of wet day precipitation intensities (Figure 6). Projected changes for the Southeast region are also negative, but small and inconsistent among AOGCMs for all metrics of the probability distribution.

[24] Projected changes in the Midwest region are consistently positive with the largest magnitude increases in the extremes (P_{90}). For both projection periods, all 10 downscaled AOGCMs indicate increases, which range from a 10-model mean of 3.2% for the 10th percentile daily precipitation accumulation, to 7.7% for the 90th percentile for 2046–2065 to 6.6% for the 10th percentile to 11.1% for the 90th percentile for 2081–2100 (Table 2). The consistency of these changes, coupled with the amplification in the upper tail of the distribution (Figure 6) reflect a positive shift in the central tendency and widening of the probability distribution for wet day precipitation intensities. The Northeast region also exhibits an overall increase in the mean wet day precipitation intensity, but it is characterized by negative tendency for small precipitation intensities, as characterized by the 10th percentile, inconsistent changes in the median wet day precipitation amount, and consistent positive changes of nearly 25% (approximately 5 mm) by 2081–2100 in the 90th percentile (Table 2 and Figure 6).

4.3. Total Seasonal Precipitation

[25] The preceding sections described changes in the precipitation occurrence and precipitation intensity derived

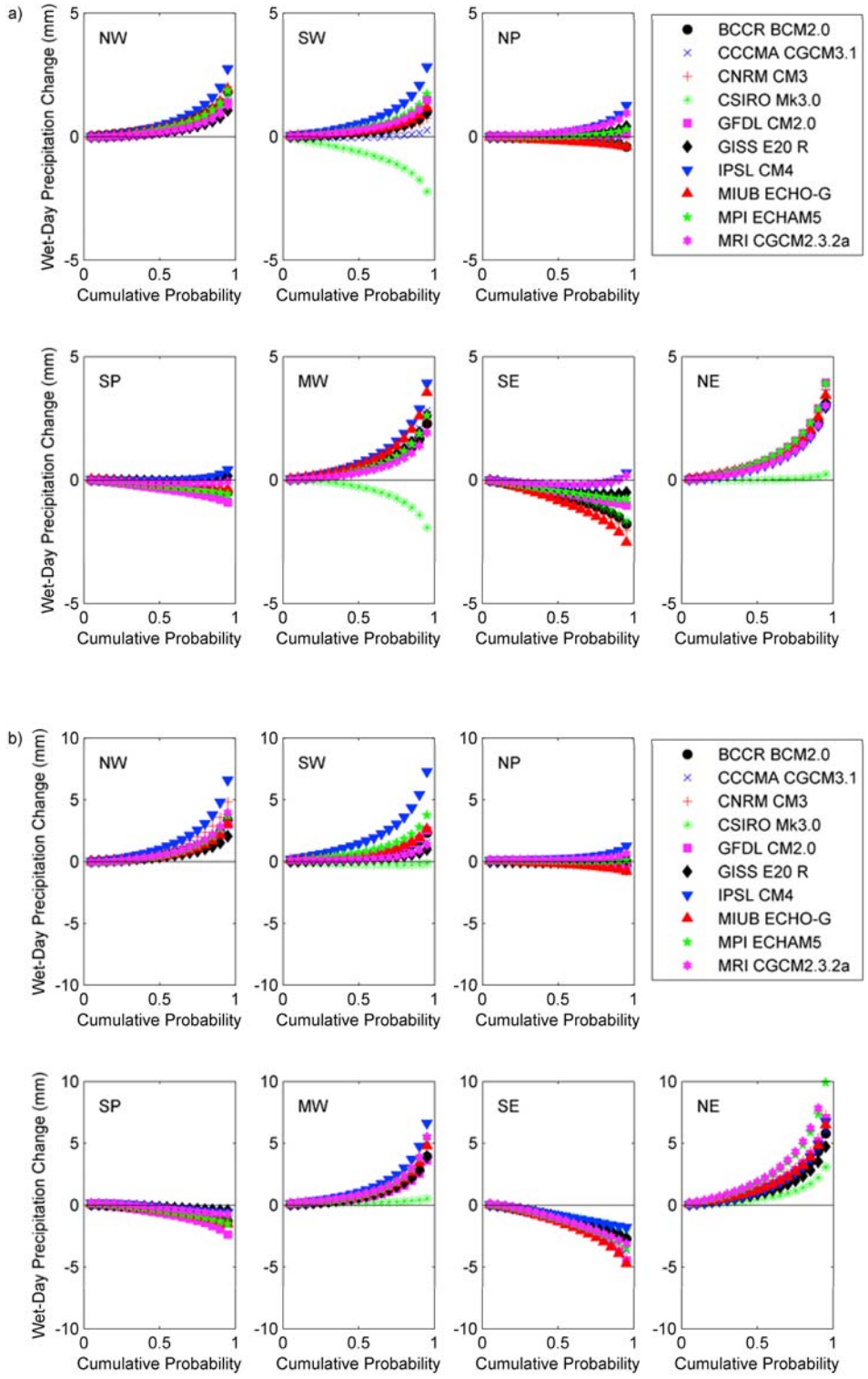

Figure 5. Projections of the change in the cumulative probability distribution of cold season (November through March) wet-day precipitation amounts for (a) 2046–2065 and (b) 2081–2100 by region. Note that the *y* axis is absolute change in precipitation (mm) and that Figures 5a and 5b have different *y* axis ranges. Values are shown for the 5th to 95th percentiles.

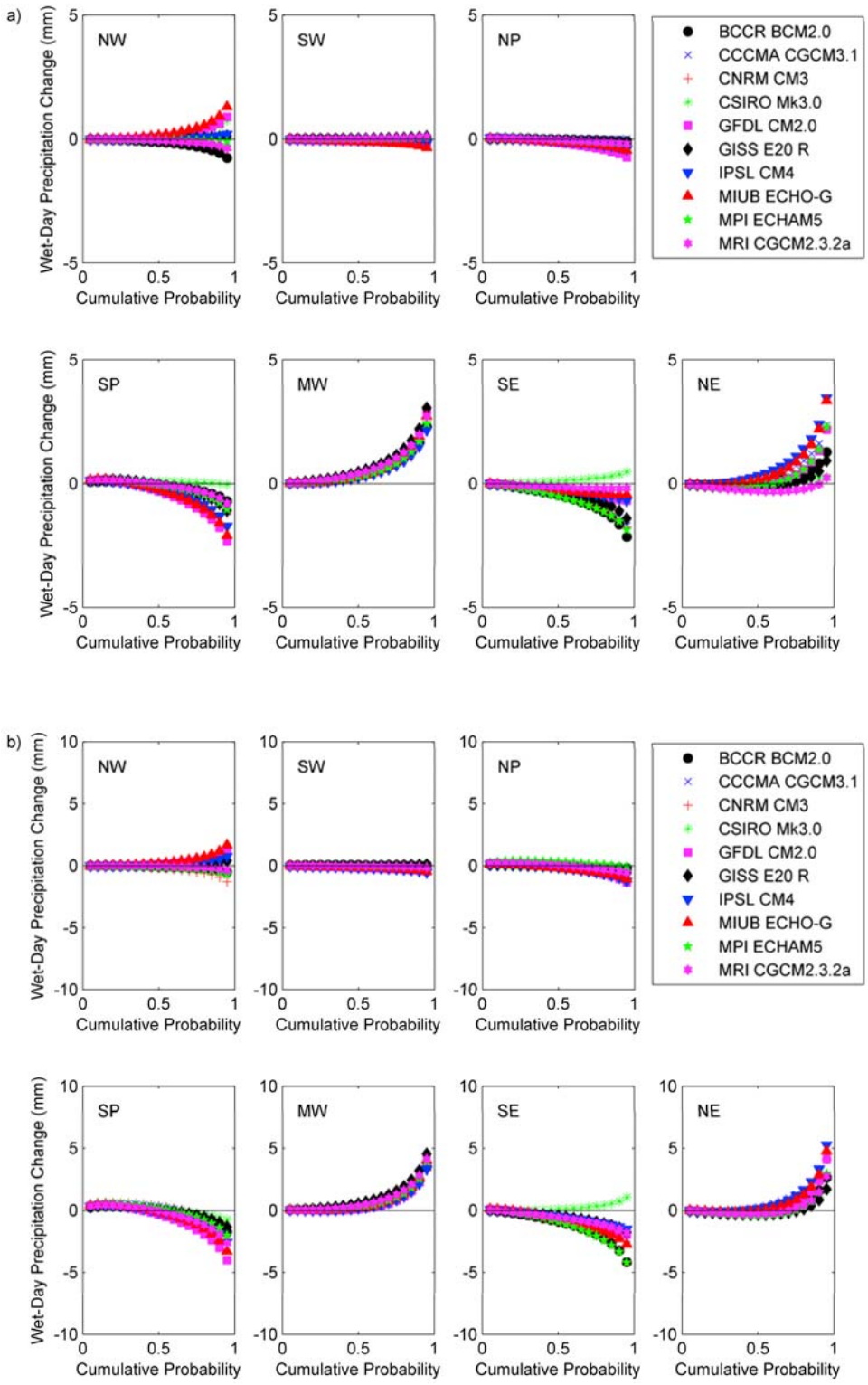

Figure 6. Projections of the change in the cumulative probability distribution of warm season (May through September) wet-day precipitation amounts for (a) 2046–2065 and (b) 2081–2100 by region. Note that the *y* axis is absolute change in precipitation (mm) and that Figures 6a and 6b have different *y* axis ranges. Values are shown for the 5th to 95th percentiles.

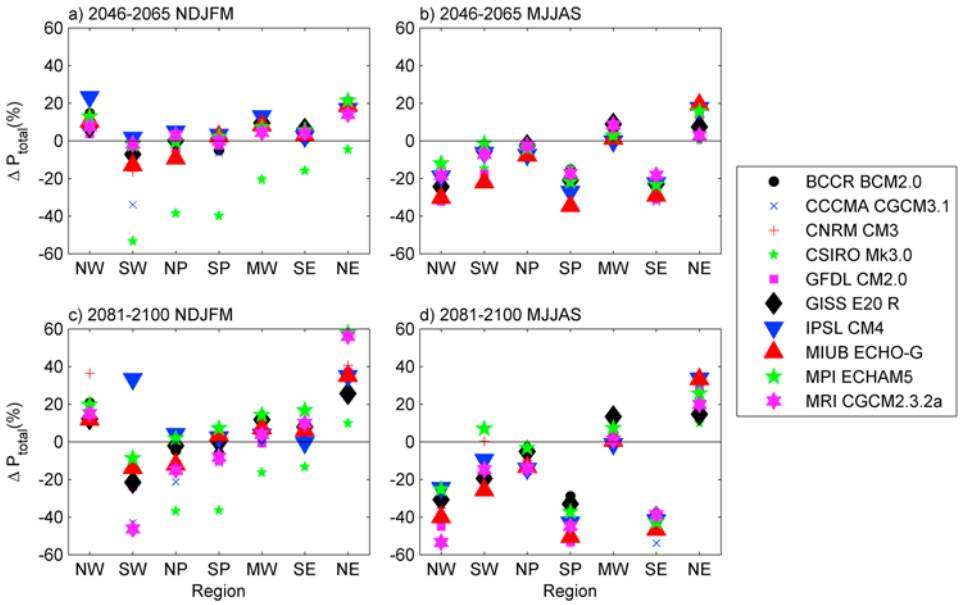

Figure 7. Projections of total seasonal precipitation change for (a, c) cold season (November through March) and (b, d) warm season (May through September) and for 2046–2065 (Figures 7a and 7b) and 2081–2100 (Figures 7c and 7d) relative to 1961–2000. Changes are shown as percentages of the 1961–2000 values averaged over all the stations in each region.

from application of statistical downscaling of 10 AOGCMs. Here we extend the analysis to total accumulated seasonal precipitation amounts and discuss the findings in terms of the projected changes in precipitation occurrence and precipitation intensity.

4.3.1. Cold Season

[26] Cold season projections for seasonal total precipitation in the Northwest and Northeast regions are characterized by large increases due to an increase in both the occurrence of precipitation and the amount of precipitation on wet days (Table 2 and Figure 7). Projected regionally averaged changes in cold season total precipitation are approximately +10% and +20% for the Northwest for 2046–2065 and 2081–2100, respectively. In this region, most of the AOGCM simulations exhibit an increase in mid-tropospheric zonal wind consistent with the poleward shift of cyclones [*Yin*, 2005]. However, the precipitation occurrence and intensity results suggest that precipitation changes in this region are primarily due to changes in intensity with an inconsistent signal for precipitation occurrence and may therefore be due to an increase in the occurrence of strong cyclones [*Christensen et al.*, 2007]. For the Northeast region, changes of approximately +15% and +35% are projected for 2046–2065 and 2081–2100 (Table 2). These changes are consistent with the westward shift in the East Coast trough [*Hayhoe et al.*, 2007].

[27] For the other five regions, projections of precipitation occurrence and intensity do not agree in sign. Changes in total seasonal precipitation therefore depend on the magnitude of these competing effects and vary from region to region. For example in the Southwest region, total cold season precipitation is projected to decrease by approximately 15% by 2046–2065 and 20% by 2081–2100 (Table 2 and Figure 7). This decrease in cold season precipitation, which is characterized by fewer, but larger events (Table 2), coupled with warmer temperatures, is consistent with changes in winter snowpack and increases in runoff as described in previous studies [*Kim*, 2005; *Leung et al.*, 2004]. Several of the AOGCM simulations are characterized by an increase in sea level pressure in the region in response to a broadening and northward displacement of the Pacific subtropical high [*Christensen et al.*, 2007]. In contrast, projections for the Southern Plains and Southeast regions are characterized by more wet days, but with smaller intensities on those days, and the projections are inconsistent between the AOGCMs in terms of the overall change in seasonal total precipitation (Table 2 and Figure 7). In the Midwest region, small decreases in precipitation occurrence are balanced by changes in precipitation intensity (especially the upper percentiles) resulting in small average changes in total cold season precipitation, though again this finding is variable with AOGCM (Table 2 and Figure 7).

4.3.2. Warm Season

[28] The downscaled AOGCM projections indicate consistent decreases in warm season precipitation throughout much of the United States, driven primarily by the decrease in precipitation occurrence (Table 2 and Figure 7). In the Northwest region, total warm season precipitation is projected to decrease by approximately 25% by 2046–2065 and 35% by 2081–2100 with a high degree of consistency among the stations within the regions and relatively little change in the distribution of wet day precipitation intensities. Changes in warm season total precipitation in the Southwest region are of smaller magnitude but also indicate declines (of over 10%) mainly due to changes in precipitation frequency. The large fractional declines in total seasonal precipitation (of over 40% by 2081–2100) in the Southern Plains and Southeast regions (Figure 7) derive

from decreases in both precipitation occurrence and precipitation intensity (Table 2 and Figure 6). Smaller decreases in warm season total accumulated precipitation in the Northern Plains are attributable to a small decline in precipitation occurrence.

[29] Despite a decrease in the number of wet days, total warm season precipitation in the Midwest region is projected to increase in most of the downscaled AOGCM simulations (Figure 7). This is partially attributable to the large increase in intense precipitation events in this region (*Pryor et al.* [2009] and Table 2). As with the cold season projections, the Northeast region is projected to experience the largest increase in total warm season precipitation, with contributions from both an increase in precipitation frequency and intensity. This finding is in contrast to prior work by *Hayhoe et al.* [2007] which projected drier summers for this region. This discrepancy may result from differences in the SRES or downscaling technique. The regional warm season results presented here for this and other regions are broadly consistent with the multimodel ensemble of *Christensen et al.* [2007].

5. Concluding Remarks

[30] In this study, we have presented a new technique for downscaling precipitation climates and developed precipitation projections for 963 surface stations across the contiguous USA using output from 10 AOGCMs. The projections were constructed by downscaling of the statistical parameters describing precipitation occurrence and intensity, using a first-order Markov chain and two-parameter gamma distribution, respectively. The downscaled model parameters were then used to derive several precipitation descriptors, including the wet day probability, the distribution of wet day precipitation intensities, and the total seasonal precipitation, which were summarized at the regional scale. Models were constructed separately for the cold season (November through March) and the warm season (May through September) with consistent predictor variables for each region studied.

[31] The precipitation projections developed in this study are characterized by several results that are robust across AOGCMs. Our results can be summarized as follows:

[32] 1. The largest total precipitation increases during the cold season occur in the Northwest and Northeast regions and are likely associated with intensification of midlatitude cyclones [*Christensen et al.*, 2007] and northward displacement of the polar jet stream and midlatitude cyclone activity [*Yin*, 2005]. The changes are characterized primarily by increases in precipitation intensity although the Northeast region is also projected to experience moderate increase in cold season precipitation occurrence. Large decreases in cold season precipitation, due to a large decrease in precipitation occurrence and despite moderate increases in wet-day precipitation intensity, occur in the Southwest region and are likely associated with expansion of the subtropical Pacific anticyclone [*Christensen et al.*, 2007]. Cold season projections for the Northern Plains region are also characterized by moderate precipitation decreases due to lower precipitation occurrence.

[33] 2. During the warm season, only the Northeast and Midwest regions are projected to experience increases in total precipitation, and in the Midwest this appears to be moderate and largely due to an increase in the magnitude of intense events. In the Northeast region, increases in large precipitation events are coupled with increases in precipitation occurrence. In each of the other regions, drier warm season conditions are projected. This decrease in warm season precipitation is principally due to a decline in precipitation frequency which is quite large for some regions (greater than 30% for the Northwest, Southern Plains and Southeast).

[34] 3. The response of total precipitation is sensitive to changes in both precipitation occurrence and precipitation intensity, underscoring the need to consider both in projections of daily precipitation evolution under climate change scenarios. The relative roles of the occurrence and intensity processes varied between regions resulting in substantive regional variations in total precipitation projections. The largest changes occur when frequency and intensity decrease or increase simultaneously, in accord with the results of *Sun et al.* [2007]. An example of the simultaneous decrease in occurrence and intensity is projected for the Southeast region during the warm season. A simultaneous increase in occurrence and intensity is projected for the Northeast region during both the cold and warm seasons.

[35] 4. The relative contributions of the precipitation occurrence and precipitation intensity processes to overall precipitation changes are sensitive to the nature of changes in wet day precipitation intensity. In cases where precipitation occurrence becomes less frequent, total precipitation can still increase if changes in the large precipitation events remain positive. An example of this type of projection occurs in the Midwest region during the warm season.

[36] 5. In general, increases in seasonal total precipitation are characterized by large positive changes in large precipitation intensities. Conversely, negative changes in precipitation receipt are characterized predominantly by large changes in small precipitation intensities with relatively little change in large events. This suggests that intense precipitation events are likely to either maintain their current frequency or increase in frequency regardless of the sign of changes in total precipitation. This result is consistent with the observational study of *Groisman et al.* [1999] and the results of the gamma distribution downscaling exercise of *Wilby et al.* [2002].

[37] This study, and the results presented in this paper are subject to several caveats. First, we employ a single greenhouse gas emissions scenario (A2). According to *Trenberth et al.* [2003], atmospheric moisture content increases at a rate of approximately 7% per K. Use of specific humidity as a predictor for many of the downscaling equations makes our analyses particularly sensitive to greenhouse gas concentrations. As an example, the warm season precipitation occurrence increases in the Southeast described in section 4.1 occur despite a general decrease in 700 mbar meridional wind, suggesting that elevated moisture availability, as manifest in the specific humidity predictor, is driving the changes. Similarly, differences between our warm season results and those of *Hayhoe et al.* [2007] for the Northeast region may be evidence of the need for additional comparisons of emissions scenarios and downscaling approaches. Second, our analysis has focused on the cold season (November through March) and the warm season (May through September). Although many impacts are directly

related to these seasonal distinctions, the climate system may also exhibit important changes in the transition seasons. For example, there is some evidence that eastern USA increases in precipitation are occurring primarily during the fall [*Small et al.*, 2006]. Third, with respect to precipitation occurrence, we have focused only on changes in the probability of precipitation occurrence. For many impacts, including those in agriculture, long spells of dry or wet days are also of importance. However, *Schoof and Pryor* [2008] demonstrated that the first-order Markov chain model used here reproduces wet and dry spells for most stations and months. Stochastic time series generation using the downscaled parameters would further facilitate analysis of variability and impact assessment and provides an avenue for further investigation. For example, changes in wet and dry spells and precipitation totals and extremes for multiday periods will be the subject of additional research. Last, changes in precipitation descriptions in some regions might be attributable to inter-decadal variations. Such variations are only considered here to the extent that they influence the large scale predictors listed in Table 1. For example, precipitation variations in the western and southern USA are partially due to variations in the Pacific Decadal Oscillation (PDO) [*Higgins et al.*, 2007]. The short (20-year) future periods used here might provide only a glimpse of a longer cycle associated with such decadal variations. Additionally, soil moisture – precipitation feedbacks may be an important regional driver of future precipitation changes, particularly in the central USA [*Koster et al.*, 2004; *Pan et al.*, 2004]. Although more work is needed to quantify the role of such feedbacks in the results presented here, it is possible that differences among the AOGCMs in terms of characterization of such feedbacks might explain some of the differences in downscaled AOGCM precipitation projections.

[38] Despite these caveats, the consistency among the downscaled AOGCMs with respect to regional precipitation evolution for several different regions and precipitation descriptors lends credence to the scenarios presented. The methodology and the results presented herein represent an advancement in the notoriously difficult problem of downscaling daily precipitation. Furthermore, the methodology described in this paper provides an avenue for further investigation of changes in the nature of fine scale precipitation under enhanced greenhouse gas forcing. An expanded application of these techniques using additional AOGCMs and forcing scenarios would further elucidate the differences among models and regions and enhance the overall confidence attached to precipitation projections.

[39] **Acknowledgments.** Support from the National Science Foundation Geography and Regional Science Program (grants 0648025 and 0647868) is gratefully acknowledged. The views expressed are those of the authors and do not necessarily reflect those of the sponsoring agency. The AOGCM data used are from the data portal developed for the 4th Assessment Report of the Intergovernmental Panel on Climate Change. We gratefully acknowledge the international modeling groups for providing their data, the Program for Climate model Diagnosis and Intercomparison for collecting and archiving the model data, the JSC/CLIVAR Working Group on Coupled Modeling and the Coupled Model Intercomparison Project and Climate Simulation Panel for organizing the model data analysis activity, and the IPCC WGI TSU for technical support. The IPCC Data Archive at Lawrence Livermore National Laboratory is supported by the Office of Science, U.S. Department of Energy.

References

Allen, R. P., and B. J. Soden (2008), Atmospheric warming and the amplification of precipitation extremes, *Science*, *321*, 1481–1484, doi:10.1126/science.1160787.

Benestad, R., et al. (2008), *Empirical-Statistical Downscaling*, 228 pp., World Sci., Singapore.

Cannon, A. J. (2008), Probabilistic multisite precipitation downscaling by an expanded Bernoulli-gamma density network, *J. Hydrometeorol.*, *9*, 1284–1300, doi:10.1175/2008JHM960.1.

Cavazos, T., and B. C. Hewitson (2005), Performance of NCEP-NCAR reanalysis variables in statistical downscaling of daily precipitation, *Clim. Res.*, *28*, 95–107.

Christensen, J. H., et al. (2007), Regional climate projections, in *Climate Change 2007: The Physical Scientific Basis*, edited by S. Solomon et al., pp. 847–940, Cambridge Univ. Press, Cambridge, U. K.

Groisman, P. Y., et al. (1999), Changes in the probability of heavy precipitation: Important indicators of climatic change, *Clim. Change*, *42*, 243–283, doi:10.1023/A:1005432803188.

Groisman, P. Y., et al. (2001), Heavy precipitation and high streamflow in the contiguous United States: Trends in the twentieth century, *Bull. Am. Meteorol. Soc.*, *82*, 219–246, doi:10.1175/1520-0477(2001)082<0219:HPAHSI>2.3.CO;2.

Groisman, P. Y., et al. (2005), Trends in intense precipitation in the climate record, *J. Clim.*, *18*, 1326–1350, doi:10.1175/JCLI3339.1.

Grotch, S. L., and M. C. MacCracken (1991), The use of general circulation models to predict regional climate change, *J. Clim.*, *4*, 286–303, doi:10.1175/1520-0442(1991)004<0286:TUOGCM>2.0.CO;2.

Hayhoe, K., et al. (2007), Past and future changes in climate and hydrological indicators in the US northeast, *Clim. Dyn.*, *28*, doi:10.1007/s00382-006-0187-8.

Haylock, M., et al. (2006), Downscaling heavy precipitation over the United Kingdom: A comparison of dynamical and statistical methods and their future scenarios, *Int. J. Climatol.*, *26*, doi:10.1002/joc.1318.

Hennessy, K. J., et al. (1997), Changes in daily precipitation under enhanced greenhouse conditions, *Clim. Dyn.*, *13*, doi:10.1007/s003820050189.

Hewitson, B. C., and R. G. Crane (2006), Consensus between GCM climate change projections with empirical downscaling: Precipitation downscaling over South Africa, *Int. J. Climatol.*, *26*, doi:10.1002/joc.1314.

Higgins, R. W., et al. (2007), Relationships between climate variability and fluctuations in daily precipitation over the United States, *J. Clim.*, *20*, 3561–3579, doi:10.1175/JCLI4196.1.

Karl, T. R., and R. W. Knight (1998), Secular trends of precipitation amount, frequency, and intensity in the United States, *Bull. Am. Meteorol. Soc.*, *79*, 231–241, doi:10.1175/1520-0477(1998)079<0231:STOPAF>2.0.CO;2.

Karl, T. R., et al. (2009), *Global Climate Change Impacts in the United States*, Cambridge Univ. Press, Cambridge, U. K.

Kharin, V. V., et al. (2007), Changes in temperature and precipitation extremes in the IPCC ensemble of global coupled model simulations, *J. Clim.*, *20*, 1419–1444, doi:10.1175/JCLI4066.1.

Kim, J. (2005), A projection of the effects of the climate change induced by increased CO_2 on extreme hydrologic events in the western U.S, *Clim. Change*, *68*, doi:10.1007/s10584-005-4787-9.

Koster, R. D., et al. (2004), Regions of strong coupling between soil moisture and precipitation, *Science*, *305*, doi:10.1126/science.1100217.

Kunkel, K. E., et al. (1998), An expanded digital daily database for climatic resource applications in the midwestern United States, *Bull. Am. Meteorol. Soc.*, *79*, 1357–1366, doi:10.1175/1520-0477(1998)079<1357:AEDDDF>2.0.CO;2.

Kunkel, K. E., et al. (2005), Quality control of pre-1948 cooperative observer network data, *J. Atmos. Oceanic Technol.*, *22*, 1691–1705, doi:10.1175/JTECH1816.1.

Leung, L. R., et al. (2004), Mid-century ensemble regional climate change scenarios for the western United States, *Clim. Change*, *62*, doi:10.1023/B:CLIM.0000013692.50640.55.

Liang, X.-Z., J. Pan, J. Zhu, K. E. Kunkel, J. X. L. Wang, and A. Dai (2006), Regional climate model downscaling of the US summer climate and future change, *J. Geophys. Res.*, *111*, D10108, doi:10.1029/2005JD006685.

Meehl, G. A., J. M. Arblaster, and C. Tebaldi (2005), Understanding future patterns of increased precipitation intensity in climate model simulations, *Geophys. Res. Lett.*, *32*, L18719, doi:10.1029/2005GL023680.

Meehl, G. A., et al. (2007), The WCRP CMIP3 multimodel dataset, *Bull. Am. Meteorol. Soc.*, *88*, 1383–1394, doi:10.1175/BAMS-88-9-1383.

Mitchell, T. D., and P. D. Jones (2005), An improved method of constructing a database of monthly climate observations and associated high-resolution grids, *Int. J. Climatol.*, *25*, doi:10.1002/joc.1181.

Nakicenovic, N., and R. Swart (Eds.) (2000), *Special Report on Emissions Scenarios. A Special Report of Working Group III of the Intergovernmental Panel on Climate Change*, 570 pp., Cambridge Univ. Press, Cambridge, U. K.

Pan, Z., R. W. Arritt, E. S. Takle, W. J. Gutowski Jr., C. J. Anderson, and M. Segal (2004), Altered hydrologic feedback in a warming climate introduces a "warming hole," *Geophys. Res. Lett.*, *31*, L17109, doi:10.1029/2004GL020528.

Peterson, T. C., and R. S. Vose (1997), An overview of the global historical climatology network temperature database, *Bull. Am. Meteorol. Soc.*, *78*, 2837–2849, doi:10.1175/1520-0477(1997)078<2837:AOOTGH>2.0.CO;2.

Pryor, S. C., and J. T. Schoof (2008), Changes in the seasonality of precipitation over the contiguous USA, *J. Geophys. Res.*, *113*, D21108, doi:10.1029/2008JD010251.

Pryor, S. C., J. T. Schoof, and R. J. Barthelmie (2005), Empirical downsaling of wind speed probability distributions, *J. Geophys. Res.*, *110*, D19109, doi:10.1029/2005JD005899.

Pryor, S. C., et al. (2009), How spatially coherent and statistically robust are temporal changes in extreme precipitation in the contiguous USA?, *Int. J. Climatol.*, *29*, doi:10.1002/joc.1696.

Rosenzweig, C., et al. (2002), Increased crop damage in the US from excess precipitation under climate change, *Global Environ. Change*, *12*, 197–202, doi:10.1016/S0959-3780(02)00008-0.

Schoof, J. T., and S. C. Pryor (2008), On the proper order of Markov chain for precipitation occurrence in the contiguous United States, *J. Appl. Meteorol.*, *47*, 2477–2486, doi:10.1175/2008JAMC1840.1.

Schoof, J. T., et al. (2007), Downscaling daily maximum and minimum air temperatures in the midwestern USA: A hybrid empirical approach, *Int. J. Climatol.*, *27*, 439–454, doi:10.1002/joc.1412.

Schoof, J. T., et al. (2009), Dynamically and statistically downscaling seasonal temperature and precipitation hindcast ensembles for the southeastern USA, *Int. J. Climatol.*, *29*, 243–257, doi:10.1002/joc.1717.

Semenov, V. A., and L. Bengtsson (2002), Secular trends in daily precipitation characteristics: Greenhouse gas simulation with a coupled AOGCM, *Clim. Dyn.*, *19*, 123–140, doi:10.1007/s0038200102184.

Small, D., S. Islam, and R. M. Vogel (2006), Trends in precipitation and streamflow in the eastern U.S.: Paradox or perception?, *Geophys. Res. Lett.*, *33*, L03403, doi:10.1029/2005GL024995.

Stehlik, J., and A. Bardossy (2002), Multivariate stochastic downscaling model for generating daily precipitation series based on atmospheric circulation, *J. Hydrol.*, *256*, 120–141, doi:10.1016/S0022-1694(01)00529-7.

Sun, Y., et al. (2006), How often does it rain?, *J. Clim.*, *19*, 916–934, doi:10.1175/JCLI3672.1.

Sun, Y., et al. (2007), How often will it rain?, *J. Clim.*, *20*, 4801–4818, doi:10.1175/JCLI4263.1.

Trenberth, K. E., et al. (2003), The changing character of precipitation, *Bull. Am. Meteorol. Soc.*, *84*, 1205–1217, doi:10.1175/BAMS-84-9-1205.

Trenberth, K. E., et al. (2007), Observations: Surface and atmospheric climate change, in *Climate Change 2007: The Physical Scientific Basis*, edited by S. Solomon et al.., pp. 237–336, Cambridge Univ. Press, Cambridge, U. K.

Uppala, S. M., et al. (2005), The ERA-40 re-analysis, *Q. J. R. Meteorol. Soc.*, *131*, 2961–3012, doi:10.1256/qj.2904.2176.

Vrac, M., and P. Naveau (2007), Stochastic downscaling of precipitation: From dry events to heavy rainfalls, *Water Resour. Res.*, *43*, W07402, doi:10.1029/2006WR005308.

Wetterhall, F., A. Bárdossy, D. Chen, S. Halldin, and C.-Y. Xu (2006), Daily precipitation-downscaling techniques in three Chinese regions, *Water Resour. Res.*, *42*, W11423, doi:10.1029/2005WR004573.

Wilby, R. L., and T. M. L. Wigley (2000), Precipitation predictors for downscaling: Observed and general circulation model relationships, *Int. J. Climatol.*, *20*, 641–661, doi:10.1002/(SICI)1097-0088(200005)20:6<641::AID-JOC501>3.0.CO;2-1.

Wilby, R. L., et al. (2002), Prospects for downscaling seasonal precipitation variability using conditioned weather generator parameters, *Hydrol. Processes*, *16*, 1215–1234, doi:10.1002/hyp.1058.

Wilks, D. S. (1992), Adapting stochastic weather generation algorithms for climate change studies, *Clim. Change*, *22*, 67–84, doi:10.1007/BF00143344.

Wilks, D. S. (1999), Interannual variability and extreme-value characteristics of several stochastic daily precipitation models, *Agric. For. Meteorol.*, *93*, 153–169, doi:10.1016/S0168-1923(98)00125-7.

Wilks, D. S. (2006), *Statistical Methods in the Atmospheric Sciences*, 2nd ed., 627 pp., Academic, San Diego, Calif.

Yin, J. H. (2005), A consistent poleward shift of the storm tracks in simulations of 21st century climate, *Geophys. Res. Lett.*, *32*, L18701, doi:10.1029/2005GL023684.

Zhang, X., et al. (2007), Detection of human influence on twentieth-century precipitation trends, *Nature*, *448*, 461–465, doi:10.1038/nature06025.

S. C. Pryor, Atmospheric Science Program, Department of Geography, Indiana University, Bloomington, IN 47405, USA.

J. T. Schoof and J. Surprenant, Department of Geography and Environmental Resources, Southern Illinois University, Carbondale, IL 62901, USA. (jschoof@siu.edu)